## **CONFERENCE PRE-PRINT**

# DEVELOPMENT OF EQUILIBRIUM CONTROL SIMULATOR AND EXPERIMENTAL VALIDATION OF ADVANCED ISO-FLUX EQUILIBRIUM CONTROL DURING THE FIRST OPERATIONAL PHASE OF JT-60SA

S. Inoue

National Institute for Quantum Science and Technology (QST)

Naka/Ibaraki, Japan

Email: inoue.shizuo@qst.go.jp

Y. Miyata, S. Kojima, T. Wakatsuki, M. Takechi, Y. Ohtani, Y. Ko, M. Yoshida, H. Urano, and T. Suzuki National Institute for Quantum Science and Technology (QST)

Naka/Ibaraki, Japan

## Abstract

A new equilibrium control scheme was developed and validated during the integrated commissioning of JT-60SA. Based on ISO-FLUX and incorporating an Adaptive Voltage Allocation (AVA) scheme, the controller dynamically distributes voltage between plasma current ( $I_p$ ) and position/shape control under power supply voltage saturation. Pre-optimized gains from the nonlinear simulator MECS worked throughout the integrated commissioning without any modification, enabling stable operation up to 1.2 MA, the highest current in a superconducting tokamak. Experiments also revealed nonlinear plasma responses, including axisymmetric resonant field amplification, in agreement with nonlinear but not linear models. These results demonstrate the necessity of nonlinear modeling for reliable prediction and robust optimization of equilibrium control in next-generation devices.

# 1. INTRODUCTION

One of the most fundamental indicator for nuclear fusion reactors is the power density, which directly reflects the efficiency of energy production within the plasma volume. The power density produced by fusion reactions is proportional to the square of the density of the ionized fuel gas and to the reaction reactivity. In the temperature range where most fusion reactions occur (10-15 keV), reactivity can be approximated as linear with respect to temperature. Under this assumption, the power density scales with the square of the plasma pressure. In magnetic confinement fusion devices, this pressure is balanced by the magnetic fields generated by external coils. Consequently, the coils represent one of the major cost components of a fusion reactor. The plasma beta, defined as the plasma pressure normalized to the combined magnetic energy of plasma and coils, serves as a key cost indicator. As beta increases, the free energy stored in the plasma grows, leading to the onset of ideal magnetohydrodynamic (MHD) instabilities. Stability analyses have shown that the achievable beta scales with the plasma current [1]. Increasing the plasma current, however, enhances the surrounding poloidal magnetic field through Ampère's law, thereby reducing the safety factor, defined as the inverse of the shear of the magnetic field line. Ideal MHD stability requires the safety factor to exceed 2, and considering operational margins, values above approximately 3 are desirable. To maintain high plasma current while simultaneously increasing the safety factor—i.e., reducing the poloidal field—it is necessary to expand the plasma cross-sectional area. Accounting for the 1/R dependence of the toroidal field, this requires elongating the plasma vertically (in the Z-direction) to achieve high elongation. High elongation thus improves fusion performance, but it also renders the plasma magnetohydrodynamically unstable. Without control, the plasma would move at approximately the Alfvén velocity, leading to loss of confinement. In practice, conducting walls slow this displacement to a timescale comparable to the wall skin time, while longerwavelength oscillations exceeding this timescale are continuously suppressed by feedback control. In other words, fusion devices achieve improved reaction rates by stabilizing an inherently unstable, high-elongation equilibrium through active control. In this sense, equilibrium control constitutes one of the most fundamental and indispensable technologies in fusion reactors.

In equilibrium control, modern control theories such as H-infinity have long been employed [2], which has motivated the use of linearized systems of equations. Within the linear framework, a proportional relationship is assumed between variations in the coil currents applied for control and the resulting plasma displacements. For

instance, in the RZIP model [3], the plasma is approximated as a line current, and its displacement is derived from the force balance of this current. A more refined representation is the so-called non-rigid model [4], in which the plasma displacement is obtained from the relationship between the perturbation of the Grad-Shafranov equilibrium and variations in the plasma current. In both cases, transient physical processes—such as the fact that the plasma can move at approximately the Alfvén velocity, with its motion constrained by eddy currents—are neglected. This coupled interaction between conducting structures and plasma motion, in which the plasma vertically displaces with a characteristic time scale comparable to the wall skin time, is referred to as a vertical displacement event (VDE) [5]. Such instabilities typically arise in plasmas with high elongation. From the standpoint of the energy principle, vertical instability (VI) manifests as the plasma evolving toward a state where the sum of its internal energy and the perturbed magnetic energy of surrounding walls and coils is minimized. The formulation of plasma energy in terms of the perturbed Grad-Shafranov equation has been rigorously established[6]. Numerical codes such as MECS [7] and DINA [8] can self-consistently simulate VI by solving the free-boundary Grad-Shafranov equation coupled with the circuit equations.

Here, we define a nonlinear model as one that can self-consistently reproduce vertical instability (VI) by solving the coupled free-boundary Grad-Shafranov and circuit equations, whereas simplified formulations such as the rigid model are referred to as linear models. The objective of this study is to clarify the differences in plasma response to vertical position control between linear and nonlinear models, and thereby to reveal the essential physics required for accurate prediction of equilibrium control, which is directly linked to improved fusion performance. In this context, we report the first identification of the nonlinear plasma response, including axisymmetric field amplification.

## 2. CONTROL MODEL

#### 2.1. Adaptive Voltage Allocation scheme

A new control scheme was developed for the JT-60SA experiment [9], which adaptively allocates power-supply voltage between position/shape (P/S) control and  $I_p$  control under saturation conditions. For completeness, we briefly review the voltage-control model, which is essential for interpreting the integrated commissioning experiments.

The equilibrium controller is based on the ISO-FLUX scheme [7]. Magnetic flux vectors  $\psi$  are defined at prescribed control points (black dots in figure 1), and are related to active coil currents  $I_c$  as

$$M\delta I_c = \delta \psi, \tag{1}$$

where M is the coil-to-flux response matrix. The coil circuit dynamics are described by

$$M_c \frac{dI_c}{dt} + \frac{d(M_p I_p)}{dt} + R_c I_c = V_c,$$
 (2)

with  $M_c$  the inductance matrix,  $R_c$  the coil resistance, and  $V_c$  the applied voltage.

By integrating (2) over one cycle  $\delta t$  and substituting (1), the control voltage is obtained as

$$V_c = M_c M^{\dagger} \frac{\delta \psi}{\delta t} + \frac{\delta (M_p I_p)}{\delta t} + R_c I_c,$$
(3)

where  $M^{\dagger}$  is the pseudo-inverse of M. When the problem is ill-conditioned, Tikhonov regularization with adaptively chosen parameters is applied [10].

The control target  $\delta \psi$  is decomposed into  $I_p$  and P/S contributions. For  $I_p$  control, variations in magnetic flux at the plasma boundary follow

$$-\frac{d\psi_X}{dt}I_p = \frac{d}{dt}\left(\frac{1}{2}L_iI_p^2\right),\tag{4}$$

where  $\psi_X$  is the LCFS flux and  $L_i$  the internal inductance. The poloidal magnetic energy is

$$W_p = \int \frac{B_p^2}{2\mu_0} dV = \frac{1}{2} L_i I_p^2.$$
 (5)

The diamagnetic diagnostic provides  $l_i \equiv 2L_i/(\mu_0 R_j)$  [11, 12], with  $R_J$  the current centroid from CCS [13]. In commissioning,  $l_i$  was fixed to 0.8 when diagnostics were not available. Any mismatch is compensated by the newly developed adaptive voltage allocation (AVA) scheme. In this scheme, the control variable for plasma current

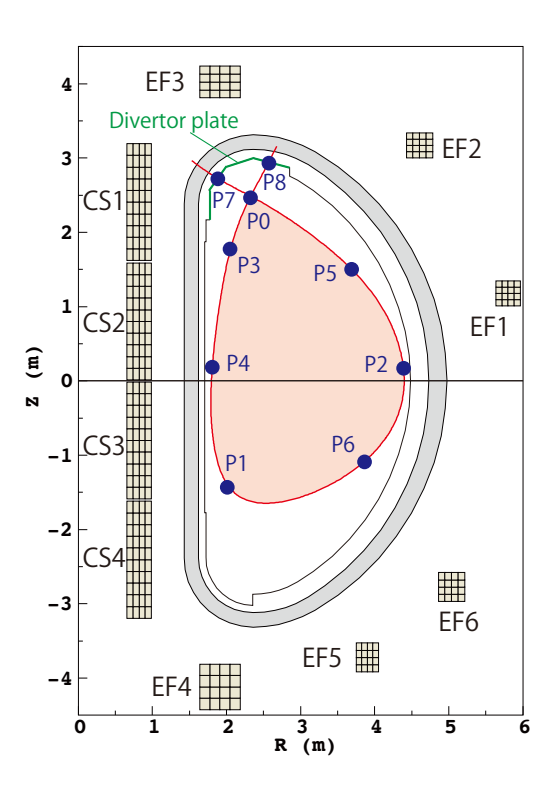


FIG. 1. Device conditions of JT-60SA during the integrated commissioning.

is adaptively adjusted so as to avoid voltage saturation, thereby mitigating interference with position and shape control. Details of the logic are presented below.

For P/S control, the control variable is

$$\delta \psi_{s} \equiv \psi_{X} - \psi. \tag{6}$$

PID controllers are applied:

$$\delta\psi_{X,\text{PID}} = G_{XP}\delta\psi_X + G_{XI}\int \delta\psi_X dt + G_{XD}\frac{d\delta\psi_X}{dt}, \tag{7}$$

$$\delta \psi_{s,\text{PID}} = G_{\text{SP}} \delta \psi_s + G_{\text{SI}} \int \delta \psi_s dt + G_{\text{SD}} \frac{d\delta \psi_s}{dt}. \tag{8}$$

An adaptive voltage allocation (AVA) gain is introduced:

$$\delta\psi_{X,\text{AVA}} = G_{X,\text{AVA}}\delta\psi_{X,\text{PID}}.$$
 (9)

 $G_{\rm X,AVA}$  is tuned in real time by binary search so that voltages approach but do not exceed supply limits. All procedures, including  $G_{\rm X,AVA}$  adjustment, are executed within the 250  $\mu$ s control cycle. The final control variable is  $\delta \psi \equiv \delta \psi_{\rm X,AVA} + \delta \psi_{\rm S,PID}$ , so all coils contribute to both  $I_p$  and P/S control.

PID gains are tuned by frequency-response analysis [14]. Perturbations of 2-25 Hz were applied to  $I_p$  and P/S references, and deviations were minimized. Remarkably, gains pre-tuned with the MECS simulator [7, 15, 16] worked throughout commissioning with little modification, confirming the validity of MECS-based tuning. Subsequent analysis [17] suggested that a slightly larger  $I_p$  P-gain improves tracking under the AVA scheme, while MECS-derived P/S gains were nearly optimal.

## 3. EXPERIMENTAL MILESTONES ACHIEVED DURING THE INTEGRATED COMMISSIONING

In the JT-60SA control system, conventional PID control with an advanced ISO-FLUX scheme [9] was adopted for both plasma current  $(I_p)$  and shape control. Figure 2 shows (a) the maximum achieved  $I_p$  and (b,c) the control

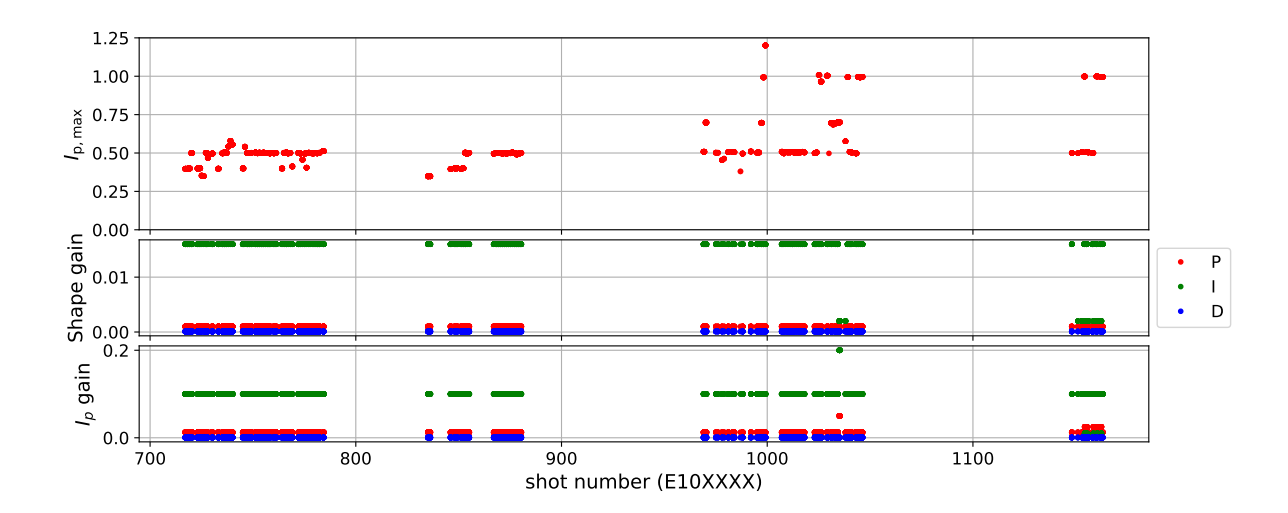


FIG. 2. (a) Maximum  $I_p$  and (b,c) control gains during IC1. The maximum  $I_p$  of 1.2 MA was achieved without gain optimization.

gains used in IC1 [18]. The horizontal axis represents the shot number, from the E100700 series (start of feedback control) to E101163. The maximum  $I_p$  exceeded 1.2 MA, setting a record for superconducting tokamaks. Despite gains being automatically plotted when  $I_p \geq 300 \, \text{kA}$ , PID gains remained constant, except for a few E101000-series shots where they were intentionally modified for gain-optimization tests. This robustness, not generally expected, was enabled by pre-optimized gains obtained with the nonlinear simulator MECS [7], which accurately reproduces plasma response to coil currents.

An Adaptive Voltage Allocation (AVA) scheme was developed to mitigate interference between  $I_p$  and shape control during elongation in  $I_p$  ramp-up. Its effects, first confirmed by MECS [7, 15], were validated in commissioning by comparing discharges with and without AVA (figure 3). In these experiments,  $I_p$  was ramped to 500 kA at 1 s, held until 2 s, then increased to 1.2 MA. Feedback control with AVA began at 1 s, while pre-programmed voltages were applied earlier. At the onset of feedback, a discrepancy between target and actual  $I_p$  was observed, accompanied by a vertical shift due to imperfect pre-programming. Once feedback began,  $G_{X,AVA}$  was reduced (figure 3(d)) to relieve voltage saturation (figure 3(c)) arising from  $I_p$ -P/S interference. Both CS and EF coils were used in  $I_p$  control, and reduction of  $G_{X,AVA}$  alleviated voltages in both. Without AVA ( $G_{X,AVA}$  = 1), oscillations appeared during  $I_p$  ramp-up from 500 to 700 kA, leading to vertical instability (figure 3(e)). With AVA, stable ramp-up to 1.2 MA was achieved, marking not only the JT-60SA record but also the world 's highest  $I_p$  in a superconducting tokamak, comparable to KSTAR [19]. Clearly, in the successful 1.2 MA discharge, the deviation between the control points and the LCFS was maintained within 2 cm during the flat-top phase, as shown in figure 3 (e). This indicates that not only the plasma current ( $I_p$ ) but also the diverted configuration was well controlled.

#### 4. RESONANT AXISYMMETRIC FIELD AMPLIFICATION

In this section, experimental data from JT-60SA during the integrated commissioning are used to explore whether the vertical oscillations of plasmas can be consistently represented by a nonlinear model or a linear model. Figure 4 shows a comparison between the experiment (E100867) and the nonlinear and linear models in MECS simulation. Vertical oscillations of the plasma were deliberately excited in response to pre-programmed variations of the EF coil current. In the MECS simulations with the linear and nonlinear models, the experimental conditions were reproduced, and only the plasma response model was varied. The nonlinear model successfully reproduced not only the amplitude but also the phase of the experimental oscillations, whereas the linear model failed to capture the observed behavior. This demonstrates the essential role of nonlinear plasma response in accurately predicting equilibrium control.

It was demonstrated that the nonlinear model reproduced the experimental results with good fidelity. However, since the experiment was carried out only at a single frequency, additional frequency scans were performed using simulations. In figure 5, sinusoidal voltages with opposite polarity were applied to the upper and lower poloidal field coils of JT-60SA, and their frequency was varied. The experimental data of IC1 is shown with error bars. Regarding the amplification factor A, defined as the vertical displacement of the plasma ( $\Delta z$ ) divided by the change in coil current ( $\Delta I$ ), the nonlinear model showed amplification at  $\omega_{\rm coil} \sim 0$ , which is revealed for the first time. Not only in A but also in the phase delay, the experimental results showed good agreement with the nonlinear model.

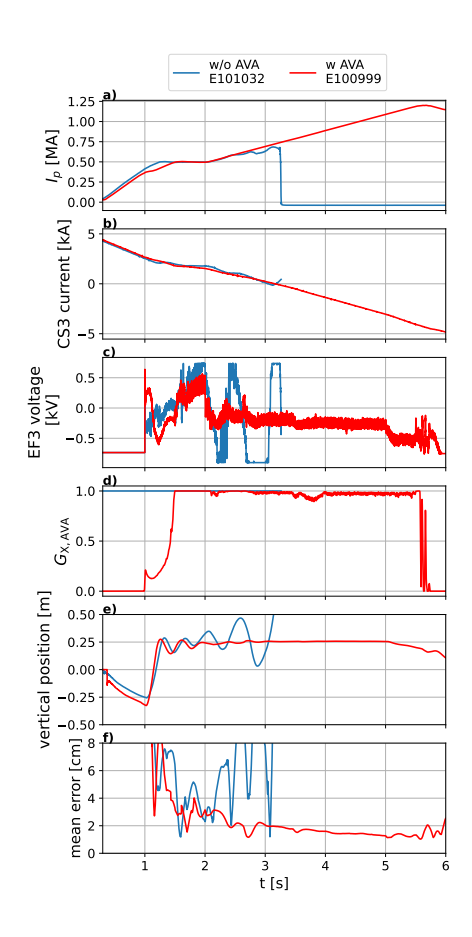


FIG. 3. Temporal evolution of a) plasma current, b,c) CS3 coil current/voltage, d)  $G_{X,AVA}$ , and e) vertical position of plasma current centroid. In E101032 (blue), AVA is off, while in E100999, AVA is active. With AVA,  $I_p$  ramped to 1.2 MA in a diverted configuration.

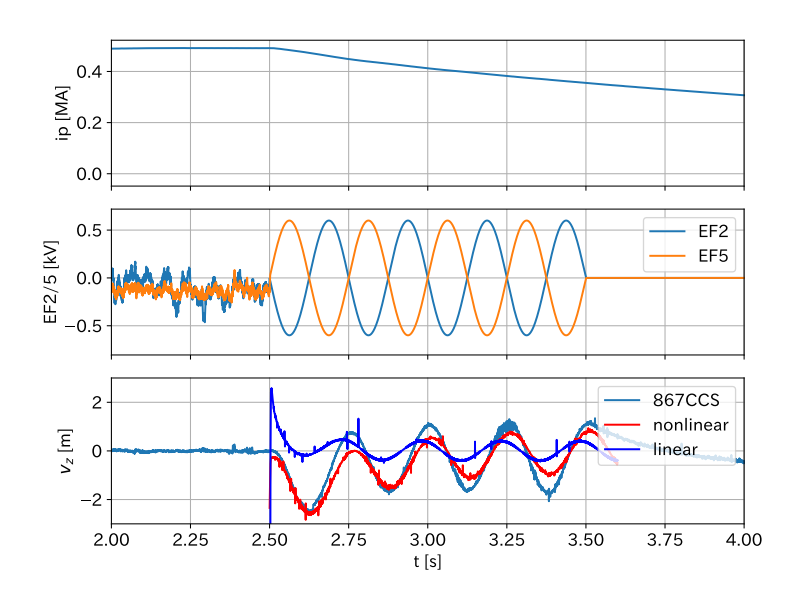


FIG. 4. Plasma vertical displacement in response to variations of EF coil current. Experimental measurements (cyan) are compared with simulations based on a nonlinear model (red) and a linear model (blue). The nonlinear model reproduces both the amplitude and phase of the experimental oscillations, whereas the linear model does not.

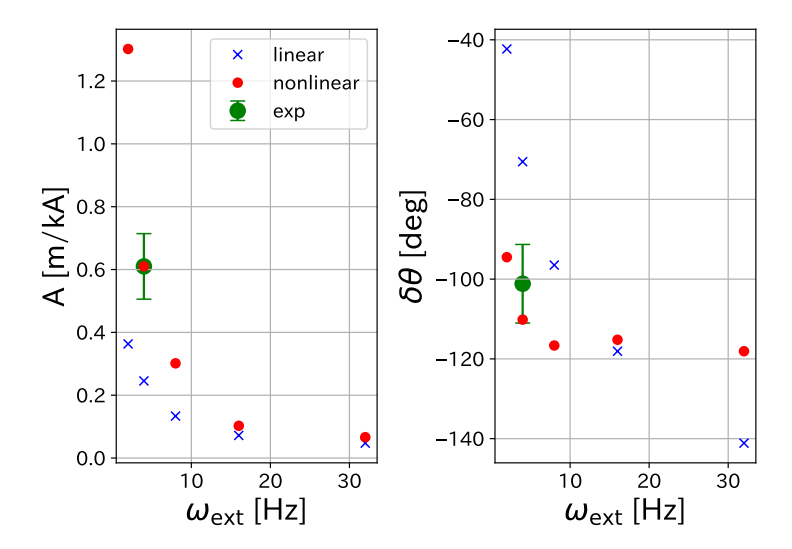


FIG. 5. Comparison of experimental results (IC1) with linear and nonlinear plasma response models. The nonlinear model reproduces both the amplification and the phase delay observed in the experiment, whereas the linear model does not.

A strong low-frequency gain observed in the nonlinear model can be interpreted as the Resonant Field Amplification (RFA) of the stable n=0 resistive wall mode. To prove this, the wall resistivity was scanned from  $0.5\eta_{\rm sus}$  to  $4\eta_{\rm sus}$  in order to explore the response in detail. Here,  $\eta_0$  denotes the original wall resistivity of stainless steel. Following the non-axisymmetric RFA formulation [20], the plasma displacement  $\delta z_s$  is related to the perturbed magnetic field  $B_s$  by introducing the 1st order lag system, as

$$\tau_W \frac{dB_s}{dt} - \gamma_0 B_s = M^* B_{\text{ext}},\tag{10}$$

where  $B_{\rm ext}$  denotes the external magnetic field including the shielding effect of eddy currents. Here we define  $B_{\rm ext0}$  as the vacuum field generated solely by the coil current variation, and assuming  $\delta z_s \sim B_s$ , the transfer function can be expressed as

$$\frac{\delta z_s}{B_{\text{ext0}}} \exp(i\delta\theta) = \frac{A_0}{(1 + i\omega\tau_W)(i\omega\tau_W - \gamma_0)},\tag{11}$$

where  $A_0$  is a constant introduced to absorb dimensional factors, and  $\tau_W$  is a wall time constant. The amplification factor is defined as the plasma vertical displacement normalized by the perturbed magnetic flux at the reference position,

$$A_B \equiv \frac{\delta z_s}{B_{\text{ext0}}}.$$
 (12)

In figure 6, the wall resistivity was varied and the responses of the linear and nonlinear models were compared. The fitting was carried out using identical parameters except for the reference wall resistivity  $\eta_0$ . It is found that the nonlinear model qualitatively reproduces the measured response with  $\tau_W = 450$  ms and  $\gamma_0 \tau_W = -20.66 \text{ s}^{-1}$ , which suggests that the observed amplification can be interpreted as the resonant field amplification.

In figure 7, the closed-loop responses obtained with the linear and nonlinear plasma response models are compared, where the proportional gain (P gain) for the plasma position and shape control system was systematically varied up to 256 times the reference value. In the linear model, the plasma remained stable up to 64× but became unstable at 256×. In contrast, the nonlinear model predicted instability already at 16×, consistent with the strong amplification due to Resonant Field Amplification (RFA). This result indicates that the frequency response of the plasma differs significantly between the linear and nonlinear regimes, implying that control gains cannot be simply scaled by a constant factor. Therefore, although computationally demanding, gain optimization with the nonlinear model is essential for reliable equilibrium control.

#### 5. SUMMARY

During the integrated commissioning of JT-60SA, an advanced ISO-FLUX equilibrium controller with an Adaptive Voltage Allocation (AVA) scheme was developed and successfully validated. The controller dynamically allocates available power-supply voltages between plasma current ( $I_p$ ) and position/shape (P/S) control, thereby mitigating

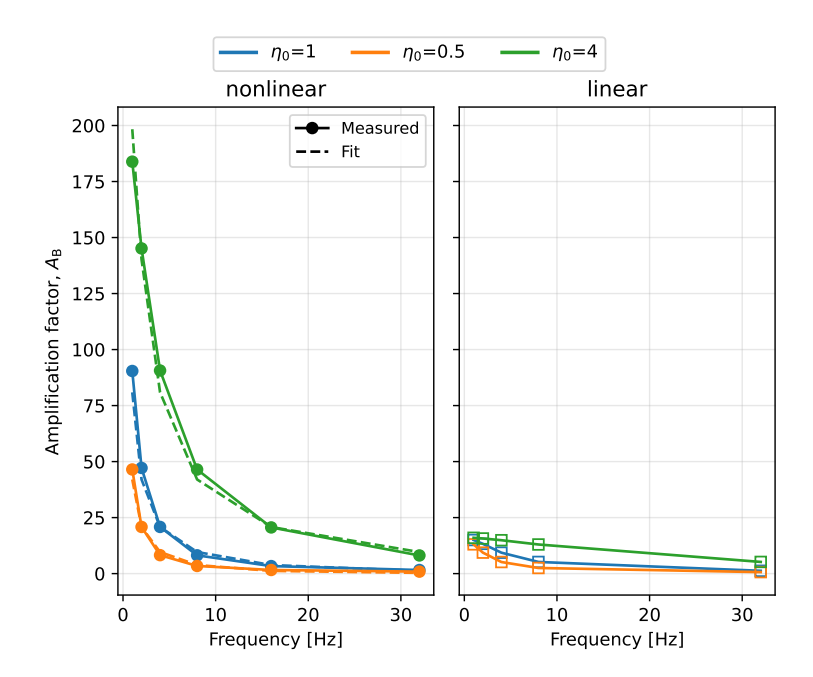


FIG. 6. Comparison of experimental results with linear and nonlinear model responses for different wall resistivities. The amplification factor  $A_B = \delta z_s/B_{\rm ext0}$  is used, and fitting was performed with identical parameters except for the reference resistivity  $\eta_0$ . The nonlinear model with the proposed first-order system including eddy-current shielding reproduces the nonlinear response.

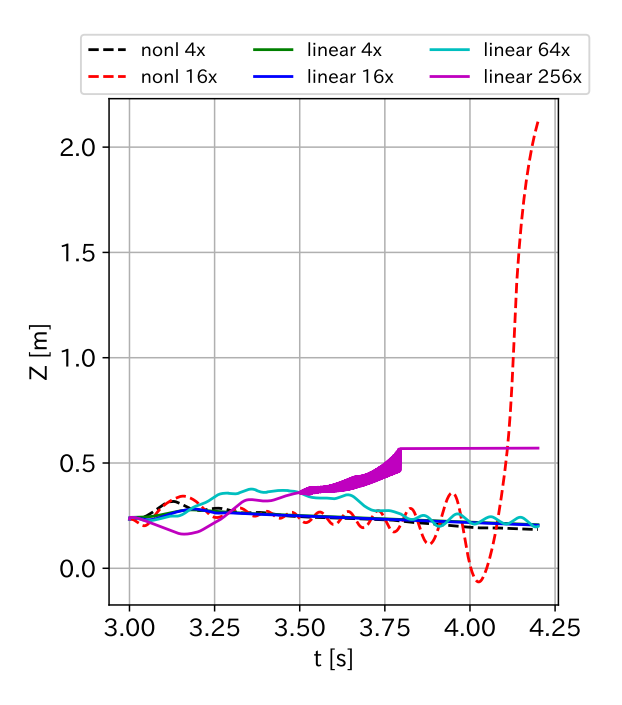


FIG. 7. Time evolution of plasma vertical displacement Z under different P gains. The linear model predicts instability at 256×, whereas the nonlinear model shows instability already at 16×, highlighting the necessity of nonlinear simulations for accurate gain optimization.

interference and saturation effects that typically occur during plasma elongation or  $I_p$  ramp-up. The control logic is executed in real time at a 250  $\mu$ s cycle, including adaptive tuning of the AVA gain, and was combined with conventional PID controllers for both  $I_p$  and P/S channels. Pre-optimized gains obtained using the nonlinear simulator MECS, which self-consistently reproduces vertical displacement events (VDEs), proved to be remarkably robust: they enabled reliable control throughout the campaign with no retuning.

As a result, JT-60SA achieved stable plasma operation up to 1.2 MA, setting a world record for superconducting tokamaks. Moreover, commissioning experiments provided the first clear identification of nonlinear plasma response, including axisymmetric resonant field amplification, which was reproduced only by nonlinear MECS simulations and not by linear models. Closed-loop tests further demonstrated that stability margins differ significantly between linear and nonlinear regimes, underscoring that gain optimization cannot be achieved by linear scaling but instead requires nonlinear modeling. These findings indicate that, in developing an equilibrium-control flight simulator, it is essential to employ a nonlinear model in order to achieve accurate prediction, which is a prerequisite for robust design and reliable operation of next-generation fusion devices.

#### REFERENCES

- [1] TROYON, F. et al., MHD-Limits to Plasma Confinement, Plasma Physics and Controlled Fusion 26 1A (1984) 209-215.
- [2] WALKER, M. L. et al., Next-generation plasma control in the DIII-D tokamak, Fusion Engineering and Design 66-68 (2003) 749-753.
- [3] COUTLIS, A. et al., Measurement of the open loop plasma equilibrium response in TCV, Nuclear Fusion **39** 5 (1999) 663–683.
- [4] PORTONE, A., The stability margin of elongated plasmas, Nuclear Fusion 45 8 (2005) 926–932.
- [5] FUKUYAMA, A. et al., Positional Instabilities in a Tokamak with a Resistive Shell, Japanese Journal of Applied Physics 14 6 (1975) 871–878.
- [6] FREIDBERG, J. P. et al., Tokamak elongation how much is too much? Part 1. Theory, Journal of Plasma Physics 81 6 (2015) 515810607.
- [7] MIYATA, Y. et al., Development of a Simulator for Plasma Position and Shape Control in JT-60SA, Plasma and Fusion Research 7 0 (2012) 1405137–1405137.
- [8] KHAYRUTDINOV, R. et al., Studies of Plasma Equilibrium and Transport in a Tokamak Fusion Device with the Inverse-Variable Technique, Journal of Computational Physics 109 2 (1993) 193–201.
- [9] INOUE, S. et al., Development of JT-60SA equilibrium controller with an advanced ISO-FLUX control scheme in the presence of large eddy currents and voltage saturation of power supplies, Nuclear Fusion **61** 9 (2021) 096009.
- [10] INOUE, S. et al., Adaptive Tikhonov regularization and dynamic control points for accurate shape parameter control of plasmas, Nuclear Fusion 64 1 (2024) 016014.
- [11] INOUE, S., Calculation of diamagnetic betap and li by using Cauchy Condition Surface scheme, Fusion Engineering and Design **168** (2021) 112401.
- [12] INOUE, S. et al., Diamagnetic energy measurements and evaluation of poloidal beta and internal inductance during the first operational phase at JT-60SA, Nuclear Fusion (2025).
- [13] KURIHARA, K. et al., The basic methods for understanding of plasma equilibrium toward advanced control, Fusion Engineering and Design **74** 1-4 (2005) 527–536.
- [14] KOJIMA, S. et al., Development of controller for fast plasma position control coils with ISO-FLUX scheme on JT-60SA, Plasma Physics and Controlled Fusion 64 11 (2022) 115007.
- [15] MIYATA, Y. et al., Study of JT-60SA Operation Scenario using a Plasma Equilibrium Control Simulator, Plasma and Fusion Research 8 0 (2013) 2405109–2405109.
- [16] MIYATA, Y. et al., Assessment of the accuracy of plasma shape reconstruction by the Cauchy condition surface method in JT-60SA, Review of Scientific Instruments 86 7 (2015) 073511.
- [17] KOJIMA, S. et al., Validation of plasma equilibrium simulator: Mecs code in jt-60sa, Proceedings of 50th EPS Conference on Plasma Physics P4-108 (2024).
- [18] INOUE, S. et al., Experimental demonstration of advanced ISO-FLUX equilibrium control during the first JT-60SA operational phase under DEMO-relevant conditions, Nuclear Fusion **65** 5 (2025) 056020.
- [19] KWAK, J.-G. et al., Kstar status and upgrade plan toward fusion reactor, IEEE Transactions on Plasma Science 48 6 (2020) 1388–1395.
- [20] REIMERDES, H. et al., Measurement of the Resistive-Wall-Mode Stability in a Rotating Plasma Using Active MHD Spectroscopy, Physical Review Letters **93** 13 (2004) 135002.